LETTERS

Anisotropy of Earth's D″ layer and stacking faults in the MgSiO₃ post-perovskite phase

Artem R. Oganov[1], Roman Martoňák[2], Alessandro Laio[2], Paolo Raiteri[2] & Michele Parrinello[2]

The post-perovskite phase of (Mg,Fe)SiO₃ is believed to be the main mineral phase of the Earth's lowermost mantle (the D″ layer). Its properties explain[1–6] numerous geophysical observations associated with this layer—for example, the D″ discontinuity[7], its topography[8] and seismic anisotropy within the layer[9]. Here we use a novel simulation technique, first-principles metadynamics, to identify a family of low-energy polytypic stacking-fault structures intermediate between the perovskite and post-perovskite phases. Metadynamics trajectories identify plane sliding involving the formation of stacking faults as the most favourable pathway for the phase transition, and as a likely mechanism for plastic deformation of perovskite and post-perovskite. In particular, the predicted slip planes are {010} for perovskite (consistent with experiment[10,11]) and {110} for post-perovskite (in contrast to the previously expected {010} slip planes[1–4]). Dominant slip planes define the lattice preferred orientation and elastic anisotropy of the texture. The {110} slip planes in post-perovskite require a much smaller degree of lattice preferred orientation to explain geophysical observations of shear-wave anisotropy in the D″ layer.

The stability and properties of the post-perovskite (pPv) phase of (Mg,Fe)SiO₃ at conditions of the Earth's D″ layer are extensively used to explain seismic features of this layer[1–4], to understand the observed geochemical anomalies[6] and global dynamics and evolution of the Earth[5,6,12]. The initial finding of pPv[1,2] was achieved with input from both experiment and theory. Here, starting from MgSiO₃ perovskite (Pv) and applying a new simulation technique[13], we obtain the pPv structure purely from first principles. This shows the potential of this simulation methodology and provides new insight into the mineralogy and physics of the Earth's D″ layer.

We use the method proposed by Martoňák *et al.*[13,14] and based on the ideas of metadynamics[15]. In this method, one introduces an order parameter—we use the lattice vectors matrix $h = (h_{11}, h_{22}, h_{33}, h_{12}, h_{13}, h_{23})$ chosen in the upper triangular form. This order parameter follows a discrete evolution:

$$h^{t+1} = h^t + \delta h \frac{\phi^t}{|\phi^t|} \quad (1)$$

where δh is a stepping parameter, and the driving force $\phi^t = -\frac{\partial G^t}{\partial \mathbf{h}}$ is calculated from the history-dependent Gibbs potential $G^t(h)$ containing gaussians added on top of the real free energy surface $G(h)$:

$$G^t(h) = G(h) + \sum_{t' < t} W e^{-\frac{|h - h^{t'}|^2}{2\delta h^2}} \quad (2)$$

where W is the height of the gaussians. The derivative of the first term on the right-hand side of (2) is:

$$-\frac{\partial G}{\partial h_{ij}} = V[h^{-1}(p - P)]_{ji} \quad (3)$$

where p is the internal pressure tensor, and P is the external pressure.

Pressure tensors are calculated from constant-*NVT* (*N*, *V* and *T* are the number of particles, volume and temperature, respectively) molecular dynamics simulations; adding gaussians (2) and evolving *h*-matrices as described above allows one to fill the free energy wells and move the system across the lowest barrier into the domain of another structure. Thus, one finds new crystal structures and structural transformation pathways, and although the latter will in general depend on the system size, precious suggestions can be inferred. To make the exploration of the free energy surface as complete as possible, it is useful to repeat simulations starting from each structure found.

We have performed classical (using a simplified interatomic potential[16] with the DL_POLY code[17]) and *ab initio* (using the VASP code[18]) simulations. While the main results discussed here were obtained *ab initio*, classical simulations were used for initial exploration of the system and for testing conditions for *ab initio* simulations (system size, run length, δ*h* and W parameters). The
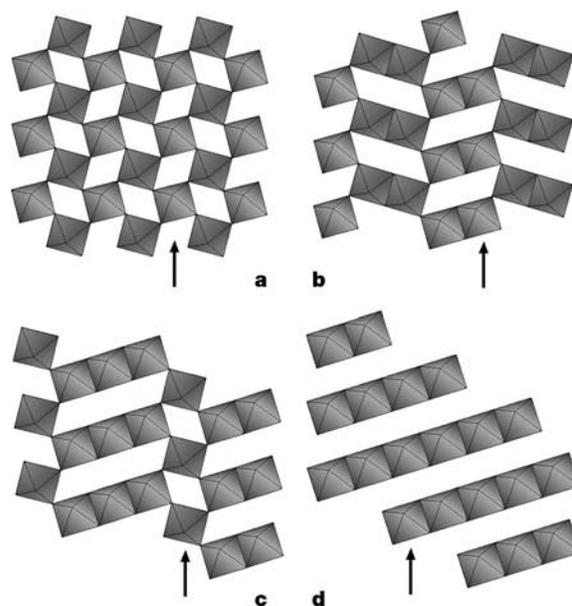

Figure 1 | MgSiO₃ polytypes found by metadynamics. a, Pv (space group *Pbnm*); **d**, pPv (*Cmcm*); **b, c**, newly found structures 2 × 2 (*Pbnm*) and 3 × 1 (*P2₁/m*), respectively. Only silicate octahedra are shown. Mg atoms are omitted for clarity. In the pPv structure, the previously expected slip plane is parallel to the sheets formed by silicate octahedra; the most likely slip plane identified here is shown by an arrow. Arrows also show slip planes in the other structures.

[1]Laboratory of Crystallography, Department of Materials, ETH Zurich, HCI G 515, Wolfgang-Pauli-Strasse 10, CH-8093 Zurich, Switzerland. [2]Computational Science, Department of Chemistry and Applied Biosciences, ETH Zurich, USI Campus, Via Giuseppe Buffi 13, CH-6900 Lugano, Switzerland.

Table 1 | **Calculated equation-of-state parameters for MgSiO$_3$ polytypes**

Phase	E_0 (eV)	V_0 (Å^3)	K_0 (GPa)	K_0'
Perovskite (*Pbnm*)	0	167.997	230.87	4.125
2 × 2 (*Pbnm*)	0.685	170.076	194.01	4.553
3 × 1 (*P2$_1$/m*)	0.645	169.563	198.55	4.515
Post-perovskite (*Cmcm*)	0.928	168.161	201.79	4.498

All results are given per 20 atoms. E_0, V_0, K_0 and K_0' are the zero-pressure energy (relative to Pv), volume, bulk modulus and its pressure derivative, respectively.

ab initio simulations were based on the generalized gradient approximation[19] and the all-electron projector augmented-wave (PAW) method[20,21]. The time step for molecular dynamics was set to 1 fs, and in classical runs we used 4 ps for equilibration and 1 ps for calculating the pressure tensor; in *ab initio* calculations 0.7 ps was used for equilibration and 0.3 ps for pressure tensor calculations. Simulated conditions are 200 GPa, 2,000 K (classical) and 150 GPa, 1,500 K (*ab initio*).

The supercells used in our calculations contained 160 atoms (4 × 1 × 2 for pPv, 2 × 2 × 2 for Pv), which is sufficiently big to encompass a large range of structures, while computationally tractable and providing clear transition paths. We used 450 eV plane-wave cut-off and the Γ-point for the Brillouin zone sampling; PAW potentials had [He] core (radius 1.52 atomic units, a.u.) for O, [Ne] core (1.5 a.u.) for Si, and [Ne] core (2.0 a.u.) for Mg. The meta-dynamics parameters we used are: δh = 1 Å and W = 38 kJ mol^{-1} in the classical case, and 0.98 Å and W = 32 kJ mol^{-1} in the *ab initio* case.

Starting from Pv (Fig. 1a), our *ab initio* simulations first found the 3 × 1 structure (Fig. 1c) and then the pPv structure (Fig. 1d). The reverse transition pathway was found in *ab initio* simulations starting from pPv. Classical simulations gave all these structures, plus the 2 × 2 structure (Fig. 1b). Table 1 reports the parameters of the Vinet equation of state[22] fitted to our *ab initio* $E(V)$ results for these phases.

It is easy to see that these phases form a continuous family: by simple sliding of the {010}$_{Pv}$ planes of the Pv structure, we can generate all the other structures. Differing only in the stacking sequence of identical layers, these structures can be described as polytypes. Polytypes had been expected[2] in pPv since its discovery, because its structure contains layers of SiO$_6$-octahedra and poly-typism is common in layered structures. However, the polytypes found here are radically different from those that were expected: they are not based on sheets of silicate octahedra parallel to {010}$_{pPv}$.

Figure 2 shows that all these polytypes become more favourable than Pv at sufficiently high pressure, but only the end members of this polytypic series, Pv and pPv, are thermodynamically stable at $T = 0$ K: Pv below 100 GPa, pPv above 100 GPa. Remarkably, the intermediate polytypes are only ~20–30 meV per atom higher in enthalpy around 100 GPa and could thus be easily stabilized by temperature and impurities and be present as minor phases in the D″ layer.

The stacking-fault enthalpy in pPv at 120 GPa is only 32 meVÅ^{-2} = 513 mJ m^{-2}, a small value similar to those found in metals at ambient pressure[23]. It is common for polytypes that their typically low-energy stacking fault planes play the role of the dominant slip planes. The {110}$_{pPv}$ slip planes at first seem counter-intuitive because they cut through the silicate sheets of the pPv structure, yet they are favourable. As shown by Legrand[23] on the example of hexagonal close-packed metals, the product of the stacking fault energy (or enthalpy) γ and the relevant shear elastic constant C_s determines the importance of a given slip plane. This criterion works very well (even though it does not explicitly account for dislocations), because it simultaneously accounts for ease of shear and formation of energetically favourable structures during plastic deformation. In our case, if the ratio $R = \frac{\gamma_{010}C_{s,010}}{\gamma_{110}C_{s,110}}$ is greater than 1, {110}$_{pPv}$ slip planes should be preferred to {010}$_{pPv}$ slip planes. By considering different types of {010}$_{pPv}$ stacking faults
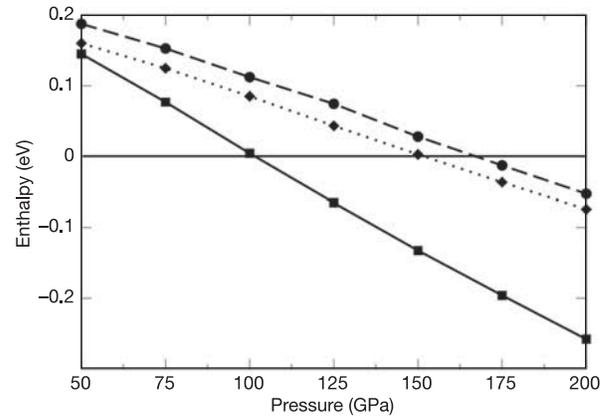

Figure 2 | **Enthalpies (relative to Pv, per formula unit) of MgSiO$_3$ polytypes as a function of pressure.** Solid line, pPv; dashed line, 2 × 2 structure; dotted line, 3 × 1 structure.

in post-perovskite, for the most stable ones (Supplementary Fig. 1) we found $\gamma_{010} = 330$ meVÅ^{-2}. Using suitably transformed elastic constants[2] we obtain $R = 9.5$ at 120 GPa, ruling out {010}$_{pPv}$ slip planes in favour of {110}$_{pPv}$ slip.

Preferred orientation along {110}$_{pPv}$ explains why in diamond-anvil cell experiments on pPv (for example, ref. 1) the {110} diffraction intensities are often vanishingly small. The fact that metadynamics could identify the most plausible slip plane in a single simulation is not surprising: the method by construction looks for the easiest non-elastic deformation mechanism and for the most energetically favourable structures along the deformation path. The mechanism of plastic deformation found here can operate also at pressures far away from the transition pressure and can be expected to be effective in analogous compounds. Indeed, using the analogy with CaTiO$_3$, Karato et al.[10] concluded that the dominant slip plane in Pv should be {010}$_{Pv}$ (in the *Pbnm* setting used also in this paper); as seen in Fig. 1, sliding {010}$_{Pv}$ planes of Pv structure produces the pPv structure. The {010}$_{Pv}$ slip was also demonstrated to be important, though not dominant, in deformation experiments[11] conducted at 25 GPa.

These {110}$_{pPv}$ slip planes in pPv call for a reinterpretation of the seismic anisotropy of the D″ layer. Using the method of ref. 24, we estimated seismic anisotropy of pPv texture with the {110}$_{pPv}$ alignment; this required the elastic constants transformed to a new coordinate system: $C'_{ijkl} = \alpha_{ip}\alpha_{jq}\alpha_{kr}\alpha_{ls}C_{pqrs}$, where α is the transformation matrix and C_{pqrs} are the elastic constants[2] in the standard setting. Convective flow in the D″ layer is inclined in the regions of subduction, vertical in upwellings, and predominantly horizontal elsewhere. Because of the positive Clapeyron slope (refs 2, 25), the pPv layer will be thicker in cold subduction regions, so if anisotropy of the D″ layer is indeed related to pPv it should be more detectable in those regions. Detailed regional studies (see refs 8, 26, 27) indicate strong $\nu_{SH}/\nu_{SV} > 1$ anisotropy with an inclined axis in subduction regions, and variable anisotropy where the flow should be horizontal. By orienting the {110}$_{pPv}$ slip planes (and the [\=110] slip directions) vertically, we find that horizontally polarized shear waves propagate 4.1% faster than vertically polarized ones ($\nu_{SH}/\nu_{SV} = 1.041$). This anisotropy is larger than the previously reported value of 2.9% calculated with the assumption of horizontally located {010}$_{pPv}$ slip planes. With the higher perfect-texture anisotropy obtained here, only 33% (65% in the regions of maximum anisotropy) alignment is required to reproduce the geophysically inferred anisotropy[9]. Orienting the slip directions at some angle (subduction angle) to the vertical would explain the inclined anisotropy invariably observed[26,27] in the regions with $\nu_{SH}/\nu_{SV} > 1$; in the regions of horizontal convective flow $\nu_{SH}/\nu_{SV} < 1$ is expected. Previous interpretations based on {010}$_{pPv}$ slip were unable to explain inclined
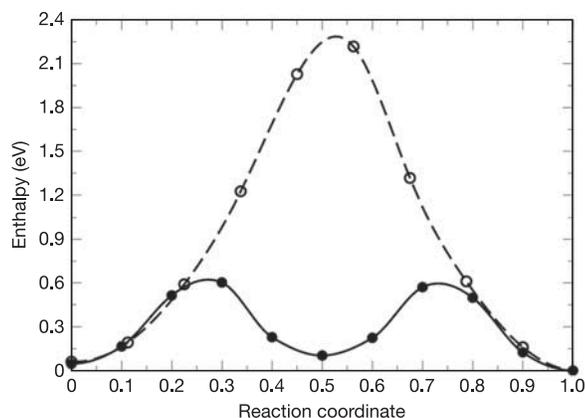
Figure 3 | Activation barrier for the Pv–pPv transition at 120 GPa. Dashed line, mechanism of ref. 25; solid line, mechanism proposed here. Enthalpies are given per formula unit. Along the reaction coordinate, the h-matrix smoothly changes from the values characteristic of Pv to those of pPv. At each point in the plot atomic positions were optimized under constraint of fixed h-matrix.

anisotropy and required unrealistically high degrees of lattice preferred orientation, 46% on average and 92% in maximally anisotropic regions.

Tsuchiya et al.[25] proposed a transition path from Pv to pPv based on shearing of the Pv structure in the $\{001\}_{Pv}$ plane. We observe this mechanism in simulations performed on a small 20-atom cell. For a larger, 160-atom system, however, we see a less cooperative mechanism with elements of nucleation: shear producing locally stacking faults with fragments of the pPv structure. First, we observe the transition from Pv to the 3×1 structure on the 15th metastep, and then to pPv on the 23rd metastep. Starting from pPv, we observe the reverse transition to perovskite following exactly the same pathway and again involving stacking faults. Using more degrees of freedom for atomic relaxation, the transition path obtained in a larger cell is by construction energetically more favourable. Direct calculation of the enthalpy as a function of the reaction coordinate (Fig. 3) shows that this effect is very large: instead of an enthalpy maximum in the middle of the transition path we have a local minimum corresponding to the intermediate 3×1 structure. As a consequence, the activation barrier at 120 GPa drops from ~2.3 eV for the pure-shear mechanism of ref. 25 to only 0.6 eV for our stacking-fault-mediated mechanism.

Our simulation technique—metadynamics—has enabled us to find the Pv–pPv transition mechanism and determine likely mechanisms of plastic deformation for both phases, involving the formation of stacking faults. Our predicted slip plane for Pv is consistent with experimental evidence. The predicted plastic slip of pPv is counterintuitive, but more consistent with geophysical observations than previous intuitive suggestions. In particular, it is now possible to explain the observed inclined character of anisotropy[26,27].

1. Murakami, M., Hirose, K., Kawamura, K., Sata, N. & Ohishi, Y. Post-perovskite phase transition in MgSiO₃. Science 304, 855–858 (2004).
2. Oganov, A. R. & Ono, S. Theoretical and experimental evidence for a post-perovskite phase of MgSiO₃ in Earth's D″ layer. Nature 430, 445–448 (2004).
3. Iitaka, T., Hirose, K., Kawamura, K. & Murakami, M. The elasticity of the MgSiO₃ post-perovskite phase in the Earth's lowermost mantle. Nature 430, 442–445 (2004).
4. Tsuchiya, T., Tsuchiya, J., Umemoto, K. & Wentzcovitch, R. M. Elasticity of post-perovskite MgSiO₃. Geophys. Res. Lett. 31, L14603 (2004).
5. Hernlund, J. W., Thomas, C. & Tackley, P. J. A doubling of the post-perovskite phase boundary and structure of the Earth's lowermost mantle. Nature 434, 882–886 (2005).
6. Ono, S. & Oganov, A. R. In situ observations of phase transition between perovskite and CaIrO₃-type phase in MgSiO₃ and pyrolitic mantle composition. Earth Planet. Sci. Lett. 236, 914–932 (2005).
7. Lay, T. & Helmberger, D. V. A shear velocity discontinuity in the lower mantle. Geophys. Res. Lett. 10, 63–66 (1983).
8. Lay, T., Williams, Q. & Garnero, E. J. The core-mantle boundary layer and deep Earth dynamics. Nature 392, 461–468 (1998).
9. Panning, M. & Romanowicz, B. Inferences on flow at the base of Earth's mantle based on seismic anisotropy. Science 303, 351–353 (2004).
10. Karato, S., Zhang, S. Q. & Wenk, H. R. Superplasticity in Earth's lower mantle—evidence from seismic anisotropy and rock physics. Science 270, 458–461 (1995).
11. Cordier, P., Ungar, T., Zsoldos, L. & Tichy, G. Dislocation creep in MgSiO₃ perovskite at conditions of the Earth's uppermost lower mantle. Nature 428, 837–840 (2004).
12. Nakagawa, T. & Tackley, P. J. Effects of a perovskite-post perovskite phase change near core-mantle boundary in compressible mantle convection. Geophys. Res. Lett. 31, L16611 (2004).
13. Martoňák, R., Laio, A. & Parrinello, M. Predicting crystal structures: The Parrinello-Rahman method revisited. Phys. Rev. Lett. 90, 075503 (2003).
14. Martoňák, R. et al. Simulation of structural phase transitions by metadynamics. Z. Kristallogr. 220, 489–498 (2005).
15. Laio, A. & Parrinello, M. Escaping free-energy minima. Proc. Natl Acad. Sci. USA 99, 12562–12566 (2002).
16. Oganov, A. R., Brodholt, J. P. & Price, G. D. Comparative study of quasiharmonic lattice dynamics, molecular dynamics and Debye model in application to MgSiO₃ perovskite. Phys. Earth Planet. Inter. 122, 277–288 (2000).
17. Smith, W., Todorov, I. T. & Leslie, M. The DL_POLY molecular dynamics package. Z. Kristallogr. 220, 563–567 (2005).
18. Kresse, G. & Furthmüller, J. Efficient iterative schemes for ab initio total-energy calculations using a plane wave basis set. Phys. Rev. B 54, 11169–11186 (1996).
19. Perdew, J. P., Burke, K. & Ernzerhof, M. Generalized gradient approximation made simple. Phys. Rev. Lett. 77, 3865–3868 (1996).
20. Blöchl, P. E. Projector augmented-wave method. Phys. Rev. B 50, 17953–17979 (1994).
21. Kresse, G. & Joubert, D. From ultrasoft pseudopotentials to the projector augmented-wave method. Phys. Rev. B59, 1758–1775 (1999).
22. Vinet, P., Rose, J. H., Ferrante, J. & Smith, J. R. Universal features of the equation of state of solids. J. Phys. Condens. Matter 1, 1941–1963 (1989).
23. Legrand, B. Relations entre la structure èlectronique et la facilitè de glissement dans les mètaux hexagonaux compacts. Phil. Mag. 49, 171–184 (1984).
24. Montagner, J.-P. & Nataf, H.-C. A simple method for inverting the azimuthal anisotropy of surface waves. J. Geophys. Res. 91, 511–520 (1986).
25. Tsuchiya, T., Tsuchiya, J., Umemoto, K. & Wentzcovitch, R. M. Phase transition in MgSiO₃ perovskite in the earth's lower mantle. Earth Planet. Sci. Lett. 224, 241–248 (2004).
26. Garnero, E. J., Maupin, V., Lay, T. & Fouch, M. J. Variable azimuthal anisotropy in Earth's lowermost mantle. Science 306, 259–261 (2004).
27. Wookey, J., Kendall, J.-M. & Rümpker, G. Lowermost mantle anisotropy beneath the north Pacific from differential S-ScS splitting. Geophys. J. Int. 161, 829–838 (2005).